Journal of Directed Energy, **2**, Fall 2007, 347–362

Comparison of Climatological Optical Turbulence Profiles to Standard, Statistical, and Numerical Models Using HELEEOS

L. E. Gravley, S. T. Fiorino,* R. J. Bartell, G. P. Perram, M. J. Krizo, and K. B. Le

Center for Directed Energy, Air Force Institute of Technology, 2950 Hobson Way, Wright–Patterson Air Force Base, Ohio 45433-7765

Optical turbulence within Earth's atmosphere plays a significant role in electromagnetic radiation propagation from a high-energy laser (HEL). The index-of-refraction structure constant, C_n^2, characterizes turbulent spatial fluctuations due to temperature gradients. These changes in the index of refraction affect the phase of the laser wavefront as it propagates through the atmosphere. It is important to characterize this parameter throughout the atmosphere, the boundary layer and above, for applications regarding emerging HEL weapons systems. Several ways to include values of optical turbulence in HEL propagation studies include standard and statistical models, physically based numerical models, and climatological compilations of observed values. The purpose here is to quantifiably compare standard, statistical, and numerical models of C_n^2 to climatological values, using the High Energy Laser End-to-End Operational Simulation (HELEEOS), to determine whether each model will yield values similar to that of actual measured optical turbulence data. The study shows that HELEEOS is a powerful tool in atmospheric optical turbulence assessment, because not only of its capability to use standard optical turbulence profiles such as Hufnagel–Valley 5/7 (HV 5/7), but also of its ability to incorporate correlated, climatologically derived turbulence profiles, a technique specifically developed for HELEEOS. The comparative analysis in this research appears to validate the HELEEOS method for correlating climatological C_n^2 to other meteorological parameters. Results illustrate that worldwide Strehl ratio estimates vary more than 10% for tactical low-altitude oblique scenarios using this technique compared to HV 5/7.

KEYWORDS: Climatology, C_n^2, Models, Optical turbulence

1. Introduction

This study examines the various methods for characterizing optical turbulence, which is significant as a quantitative comparison has never been made between the numerous standard (STD), statistical (STAT), and numerical (NUM) models and actual climatological

Received February 22, 2007; revision received September 12, 2007.
*Corresponding author; e-mail: steven.fiorino@afit.edu.

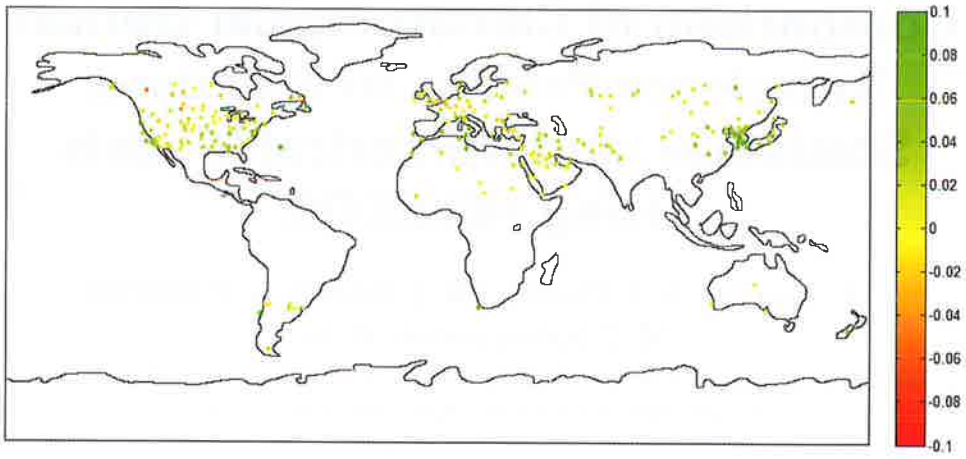

Fig. 1. Difference in Strehl ratio between HV 5/7 and the CLIM profiles for the 10th-percentile RH, winter season, a 10,000-m slant range, and 1.06-μm laser wavelength. The color bar distinguishes the difference in Strehl ratio (CLIM – HV 5/7) as a function of location.

optical turbulence. It also examines the changes in simulations of high-energy laser (HEL) system performance based on the differences in modeled index-of-refraction (C_n^2) profiles. The index-of-refraction structure constant C_n^2 characterizes turbulent spatial fluctuations due to temperature gradients, which affect the phase of the laser wavefront as it propagates through the atmosphere. A good example of these worldwide variations in system performance between simulations using different C_n^2 profiles, characterized by the ratio of atmospherically attenuated propagation to that of diffraction-limited propagation, or overall Strehl ratio, is illustrated in Fig. 1. Green sites indicate scenarios where the climatological profile produced a higher Strehl ratio than the Hufnagel–Valley 5/7 (HV 5/7) profile with a maximum difference of 0.1, and red sites indicate scenarios where the climatological profile produced a lower Strehl ratio with a maximum difference of 0.1. Figure 1 shows that a HEL weapons planner would be forced to account for a significant worldwide variation in system performance simply on the basis of the optical turbulence profile used in the calculation for the given scenario.

Various approaches to estimate the magnitude of optical turbulence vertical profiles are suitable for realistic modeling and simulation. These methods include calculations from STD, STAT, and NUM models or modified climatologies. Examples of the various STD models, which are the simplest of the three, are the HV 5/7 and the Critical Laser Enhancing Atmospheric Research (CLEAR1) models. STAT models produce mathematically generated optical turbulence profiles based on observations in climatology. NUM optical turbulence models utilize standard meteorological data to produce C_n^2 profiles via empirical or physical relations. Examples of this type of model include the Directed Energy Environmental Simulation Tool (DEEST) and the Navy Surface Layer Optical Turbulence (NSLOT) model. A modified optical turbulence climatological model is a simulation model that accesses raw climatologies of C_n^2 and correlates these data to other meteorological parameters for use in modeling and simulation. The High Energy Laser End-to-End Operational Simulation (HELEEOS) is an example of an engagement simulation that provides a modified, or correlated, C_n^2 climatology (CLIM) as an available option.

This research quantifiably compares STD, STAT, NUM, and CLIM optical turbulence models to one another and demonstrates the effects that differences have on HEL system propagation performance. The HELEEOS model is used in this study because it contains most of these various optical turbulence profiles and modeling methods as an integral part of its programming. The main function of HELEEOS is to model HEL system performance under various atmospheric conditions. It has the capabilities to model the irradiance delivered to a target considering molecular and aerosol absorption and scattering, clouds, and rain on a propagating laser wavefront and then utilizes this output to estimate the probability of a desired effect or the related parameters of required dwell time, effective range, and Strehl ratio. Aside from actual values of C_n^2, the primary comparison metric in this study is the Strehl ratio. In general, higher Strehl ratios, values closer to 1, mean shorter required dwell times and longer effective ranges.

2. Optical Turbulence Models

Three varieties of optical turbulence models are utilized by the Department of Defense. These types are the STD, STAT, and NUM models. Each has its own unique set of input parameters and equations used to calculate C_n^2. STD models are relatively simple ones that calculate optical turbulence using an analytical equation or set of equations. These models consist of one equation or a system of equations that are derived by fits to thermosonde or stellar scintillometer data. There are only a few input parameters for these calculations, which include values such as altitude, pressure level, or sometimes wind speed. Instead of capturing all of the vertical fluctuations of C_n^2 within a given profile, STD models provide a smooth and generalized trendline. Specific examples of this type of model that are used in this research are HV 5/7[7] and CLEAR1.[2]

Alternatively, STAT models are purely mathematical representations of optical turbulence profiles. Within the bounds of observations and climatology, they produce physically realistic turbulence spectra using random number generation, Monte Carlo, or other mathematical techniques. Given that observed optical turbulence profiles are not smooth functions with altitude, STAT models attempt to capture these realistic fluctuations in C_n^2. The STAT model used for this research is a toolbox called ATMtools.[1]

The NUM model DEEST consists of a collection of various models that are used to simulate optical atmospheric effects. From user input values, DEEST is able to implement specific models from its database and produce the results on an interactive display. The models that are used to produce optical turbulence profiles for a specific atmospheric layer are shown in Table 1.[8]

Table 1. DEEST C_n^2 models and their regions of applicability (adapted from Ref. 8)

Region	C_n^2 Model
Above MM5 model top (20–30 km)	CLEAR1
Above boundary layer and below MM5 model top (1–20 km)	Dewan
Within boundary layer and above surface layer (0.1–1 km)	Kaimal (unstable) or Dewan (stable)
Surface layer (0–0.1 km)	Over land: Tunick Over water: Frederickson and Davidson

The other NUM model used in this study is the NSLOT model, which was developed by Frederickson and Davidson.[5] It uses a bulk model developed from Monin–Obukhov similarity theory (MOS) and utilizes measured environmental parameters to characterize atmospheric optical turbulence and gradient properties near the ocean surface. According to MOS theory, atmospheric conditions are assumed to be horizontally stationary and homogeneous and turbulent fluxes of momentum, sensible heat, and latent heat are assumed to be vertically constant within the surface layer. The NSLOT model is a successor to the Frederickson and Davidson model utilized by the DEEST.

The tool used to analyze the data in this study is the HELEEOS model, a parametric one-on-one engagement level model, which was developed by the Air Force Institute of Technology's (AFIT) Center for Directed Energy and sponsored by the High Energy Laser Joint Technology Office (JTO). This model incorporates scaling laws tied to respected wave optics code and all significant beam degradation effects from thermal blooming due to molecular and aerosol absorption and scatter to optical turbulence. HELEEOS evaluates the uncertainty in low-altitude HEL engagement due to all major clear-air atmospheric effects as well as clouds, rain, and fog. Worldwide seasonal, diurnal, and geographical spatial–temporal variability in parameters such as temperature, pressure, water vapor content, aerosol distributions, and optical turbulence profiles is organized into probability density function (PDF) databases. To do this, HELEEOS uses a variety of resources, which include Extreme and Percentile Environmental Reference Tables (ExPERT), the Master Database for Optical Turbulence Research in Support of Airborne Laser, and the Global Aerosol Data Set (GADS).[9] Updated ExPERT mapping software allows the user to select a specific site, regional surface, and upper air data to characterize the atmospheric degradations on the beam by surface-level relative humidity (RH) percentile. Also, the PDF nature of HELEEOS's atmospheric effects package provides realistic analyses of uncertainties in the probability of desired effect. The user can access, display, and export atmospheric data independent of a HEL engagement simulation.[4]

The CLIM optical turbulence profiles in HELEEOS were developed from the data collected in the Master Database for Optical Turbulence Research in Support of Airborne Laser.[3] This database was obtained from thermosonde vertical profile measurements at different locations worldwide. For HELEEOS, the climatological values of C_n^2 were analyzed by breaking up the atmosphere into altitude layers within the planetary boundary layer and the overlying free atmosphere and obtaining C_n^2 distributions within these layers. In the boundary layer HELEEOS uses an empirical relation between C_n^2 and RH, and for the free atmosphere it relates optical turbulence to temperature for a respective altitude bin.[4] Table 2 is a visual aid to clarify how the data were categorized into the bins for each of the different atmospheric layers.

To produce a CLIM optical turbulence profile, HELEEOS begins by utilizing the ExPERT database, and with the data provided, it calculates temperature and RH profiles. It then references the lognormal distribution database and produces a mode C_n^2 value for the corresponding atmospheric bin. For the boundary layer, it produces an optical turbulence value from the altitude and RH bin that corresponds to the weather data from the ExPERT site. To produce values for the upper-air region, HELEEOS matches a C_n^2 value to the corresponding altitude and temperature bin.[4]

3. Methodology

Several tasks were accomplished for this research. The correlated C_n^2 climatology data in the CLIM model were expanded within the boundary layer and in the lower free atmosphere

Table 2. In the boundary layer, data sorted by altitude, RH range, and the corresponding optical turbulence values (top); upper-air data sorted in similar fashion, but by temperature (bottom) (adapted from Ref. 6)

0–5% RH	5–10% RH	10–15% RH	~~	95–100% RH
Altitude	Altitude	Altitude	~~	Altitude
Boundary layer	Boundary layer	Boundary layer	~~	Boundary layer
C_n^2	C_n^2	C_n^2	~~	C_n^2
−70 to −60°F	−60 to −50°F	−50 to −40°F	~~	+90 to +100°F
Altitude	Altitude	Altitude	~~	Altitude
Free atmosphere	Free atmosphere	Free atmosphere	~~	Free atmosphere
C_n^2	C_n^2	C_n^2	~~	C_n^2

to better capture low-altitude C_n^2 behavior and to accurately model optical turbulence profiles for various boundary-layer heights. Then, HELEEOS's CLIM and the STD models were compared to climatological thermosonde data, so that the differences between the profiles could be quantified and the validity of these profiles could be ascertained. Next, the STD and CLIM profiles were statistically modified using the STAT model to randomize the optical turbulence values of each one, so that the randomizations could be compared to the climatological thermosonde data. Statistics were used to quantify the differences between the STAT model randomizations and the climatological thermosonde data. The final task was to compare the numerical profiles produced by DEEST and NSLOT to the HELEEOS CLIM model to determine how well these models compare to one another.

Validation of the HELEEOS CLIM model was done by recreating the atmospheric conditions from the thermosonde campaign database and comparing the CLIM-produced C_n^2 profiles to all the corresponding thermosonde campaign C_n^2 profiles. This allowed a comparison/contrast study of the CLIM model data with the STD profiles and the thermosonde data. Further comparisons were then made to the statistical C_n^2 realizations and to numerically produced optical turbulence profiles using the NUM models, DEEST and NSLOT.

4. Results and Analysis

4.1. Model comparisons

STD models are the most widely used in the Department of Defense to characterize optical turbulence profiles. Since they are the simplest of the three types examined in this study, they are easy to use, but the curves capture only the most basic trends in the C_n^2 data and do not provide an assessment of observed optical turbulence fluctuations.

Shown in Fig. 2 are selected comparisons between the CLIM profiles produced by HELEEOS and these STD models. At the surface, the 50th-percentile midlatitude summer profile is about half the value of HV 5/7, but at approximately 300 m, they are very similar in magnitude and shape. On the other hand, the 50th-percentile midlatitude winter profile is three-and-a-half times greater than HV 5/7 at the surface and remains greater than HV 5/7 throughout the boundary layer. As for the 50th-percentile desert summer profile, the HV 5/7 profile is 50% greater than the CLIM profile, but at approximately 400 m, the CLIM profile stays about an order of magnitude greater than the other for the remainder of

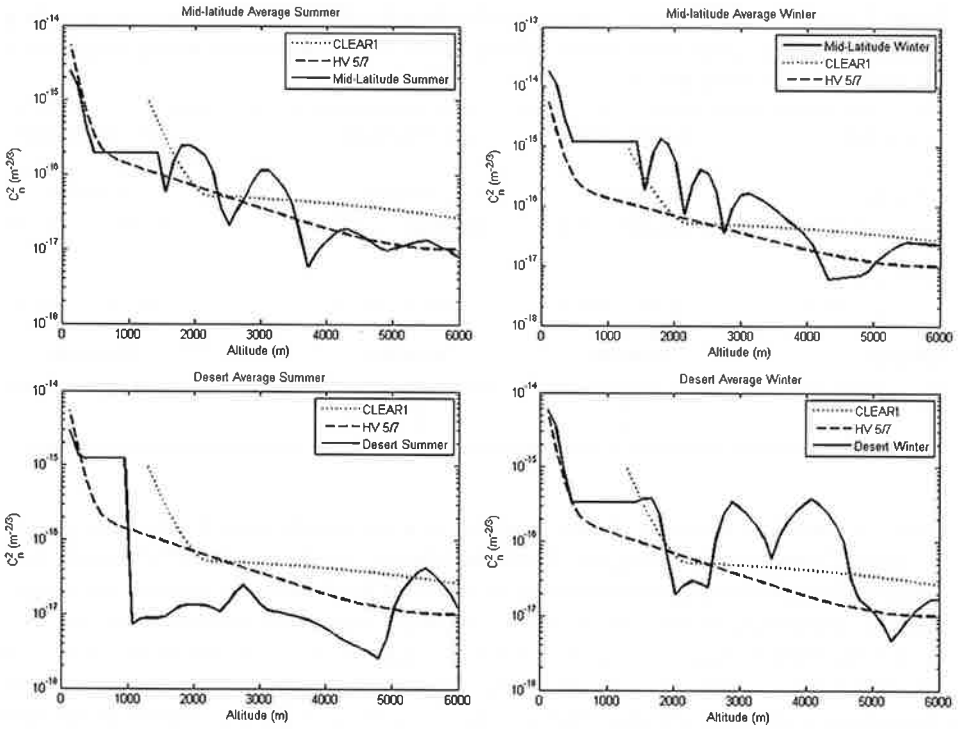

Fig. 2. Comparisons of the HELEEOS CLIM profiles for the 50th-percentile RH with the standard models of HV 5/7 and CLEAR1; midlatitude summer (top left), midlatitude winter (top right), desert summer (bottom left), and desert winter (bottom right). The boundary-layer height for the profiles is 1,525 m. Note that the midlatitude winter C_n^2 scale differs from the others and the CLEAR1 profile is not valid below 1,361 m.

the boundary layer. The 50th-percentile desert winter profile and HV 5/7 profiles compare very well throughout the boundary layer, so the HV 5/7 profile is a good estimate of a desert winter 50th-percentile RH C_n^2 profile.

The differences in optical turbulence due to the change in season can be explained by nighttime radiative transfer properties because thermosonde profiles are obtained at night to avoid solar contamination of the data. Radiation from the Earth's surface and lower atmosphere generally tends to radiate away from the Earth toward space. Since the Earth's surface and lower atmosphere are warmer and contain more water vapor during the summer, the radiation does not propagate as easily through to the top of the atmosphere. This results in more evenly distributed energy, which leads to smaller temperature gradients and smaller optical turbulence values. During the winter months, the ground and air are colder and contain less water vapor. Therefore, larger amounts of radiation can escape into space, a phenomenon that magnifies the radiative efficiencies of different surfaces. Thus, energy is less evenly distributed throughout the lower atmosphere, with larger temperature gradients and, in turn, larger C_n^2 values.

The next goal was to observe the kind of optical turbulence distributions the STAT model produced against the CLIM model output. To make the best possible comparison, conditions similar to that of the thermosonde distributions were closely mimicked for the

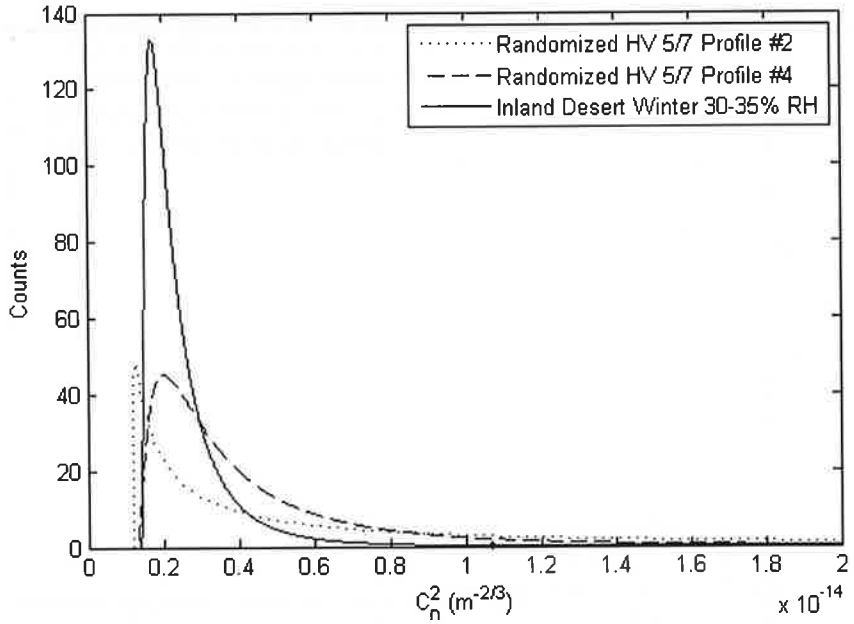

Fig. 3. Two randomized HV 5/7 C_n^2 distributions and the 30–35% RH distribution for a desert winter location (boundary layer).

Table 3. Statistics for each lognormal distribution ($m^{-2/3}$)

Parameter	Randomized profile 2	Randomized profile 4	Desert winter 30–35% RH
Area under the curve	1.05*E*–13	1.42*E*–13	1.59*E*–13
Mode value	1.26*E*–15	2.04*E*–15	1.75*E*–15
Median value	1.06*E*–14	1.06*E*–14	1.07*E*–14
Mean value	5.60*E*–15	4.36*E*–15	2.56*E*–15

input parameters to the STAT model. Using an identical boundary-layer-altitude bin as one of those defined for the HELEEOS CLIM model, the HV 5/7 and CLEAR1 profiles were statistically randomized, and the distributions were calculated (Fig. 3).

Since the distributions are calculated from the same vector size, the area under each curve is approximately the same. Each distribution has its own set of statistics, which are displayed in Table 3. The areas under each curve are approximately equal to one another, which is what one would expect with similar distribution sizes. Also, the median values are equal because of the distribution boundaries. For these distributions, the right end point is $2.0E^{-14}$ $m^{-2/3}$ and the left is approximately $1.0E10^{-16}$ $m^{-2/3}$ and therefore, the median value is half the distance between the end points. The mode values are close to one another, and the difference between them can be seen in the peaks of each plot. However, the magnitude of the desert mode is approximately three times greater than the magnitudes of the randomized

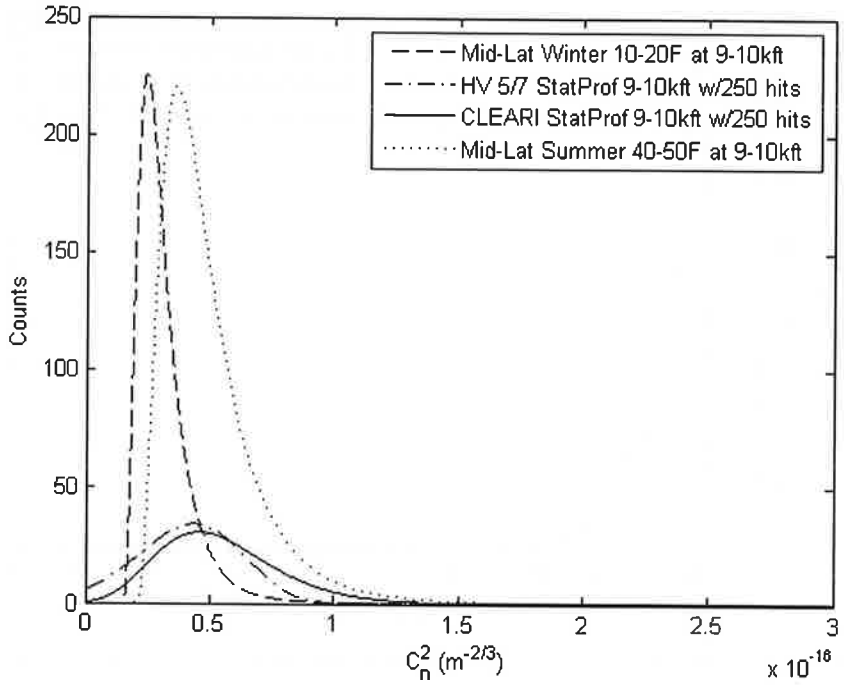

Fig. 4. Randomized HV 5/7 and CLEAR1 profiles with East Asia winter at 10–20°F and East Asia summer at 40–50°F from 9 to 10 kft (free atmosphere).

distributions. As for the mean, these values are the farthest apart, and the difference can also be seen in Fig. 3.

The next distribution comparison is between the randomized CLEAR1 and HV 5/7 and two midlatitude CLIM profiles in the free atmosphere above the boundary layer. The commonalities between them are the altitude layer, 9–10 kft, and the number count. As one can see from Fig. 4, the climatological distributions are approximately six times greater in magnitude than the Gaussian distributions. Another feature is the shape of the lognormal curve in contrast to the Gaussian distribution. A lognormal curve is a skewed Gaussian, and the degree of this feature is clearly illustrated in Fig. 4.

Comparing the distributions of C_n^2 values helps to determine whether the STAT model is realistically randomizing them. The distributions of the STAT model in the boundary layer are the most similar to the climatological distributions because they are skewed Gaussians. However, the distributions for the STAT model in the free atmosphere are normal Gaussians, and they do not mimic climatology. The smaller number counts for the mode values of the CLEAR1 and HV 5/7 profiles are most likely a consequence of the profiles' shape. Also, the magnitude of the variations in C_n^2 is much less than the physical variation. Since the statistically generated distributions are slightly different from the climatological ones, it is important to observe the STAT profile trend against the physical one. Therefore, five randomized profiles based on a midlatitude summer CLIM profile with several of the corresponding thermosonde launches were plotted together, and this relationship can be seen in Fig. 5. The blue lines represent the randomized realizations of the CLIM profile, and one can discern that the distribution about the original profile, the black line, is Gaussian-like. However, a

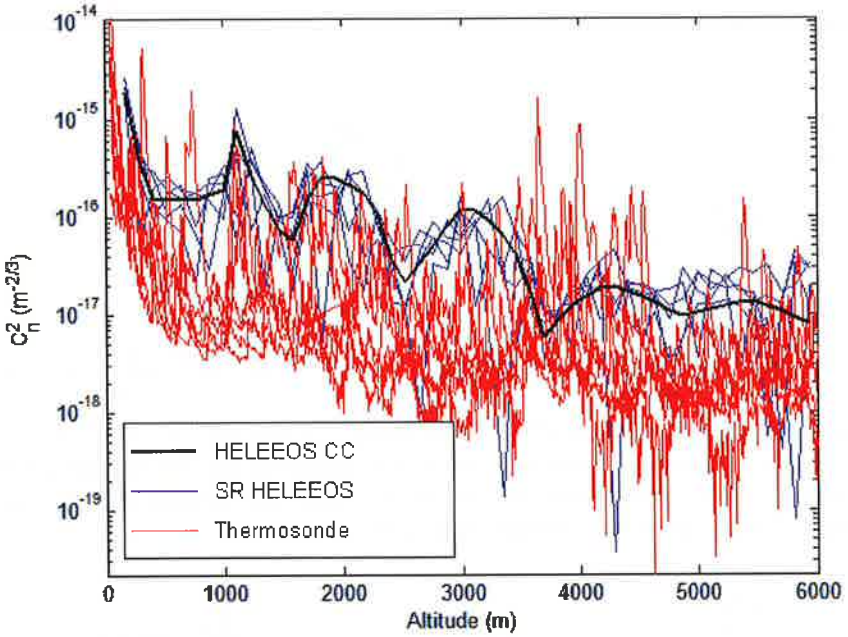

Fig. 5. Randomized midlatitude summer CLIM profile (labeled SR HELEEOS) with the corresponding East Asia thermosonde profiles. The bold black line is the unrandomized CLIM profile (labeled HELEEOS CC).

few values stray from the normal distribution, and two of them are approximately an order of magnitude smaller than the lowest thermosonde C_n^2 values. The lognormal nature of the thermosonde data is also clearly evident in Fig. 5. It has a lower, more populated baseline (in the range of 10^{-18} and 10^{-17} $m^{-2/3}$) with significant fluctuations in C_n^2, which are larger in magnitude than the base.

The differences between HV 5/7, the HELEEOS CLIM, and selected DEEST profiles are depicted in Fig. 6. The meteorological data driving the DEEST profiles comes from Air Force Weather Agency Mesoscale Model #5 (MM5) data for specified East Asia and desert summer locations, which are comparable in scenario to the thermosonde launches, except for the specific launch dates. As is evident in Figure 6, the DEEST profile is much larger than the HELEEOS CLIM and HV 5/7 profiles by two to three orders of magnitude. Shown previously in the Fig. 5 comparison to actual thermosonde data, the CLIM profile represents the high end of the observed thermosonde data rather well, even though it predicts slightly larger C_n^2 values than the standard deviation at times. Therefore, the DEEST profile is likely several orders of magnitude greater than the physical data.†

The next comparison was made between the HELEEOS CLIM and NSLOT profiles for corresponding midlatitude summer coastal land and adjacent sea locations. This is illustrated in Fig. 7 for Pyongtaek, Korea, and the nearby Yellow Sea. This particular comparison shows that both HV 5/7 and the CLIM values are the same order of magnitude as the NSLOT value

†Soon after this research was completed in late 2005, a low-altitude correction was implemented in DEEST that greatly reduces the differences in the profiles (G. Jumper, personal communication, 2007).

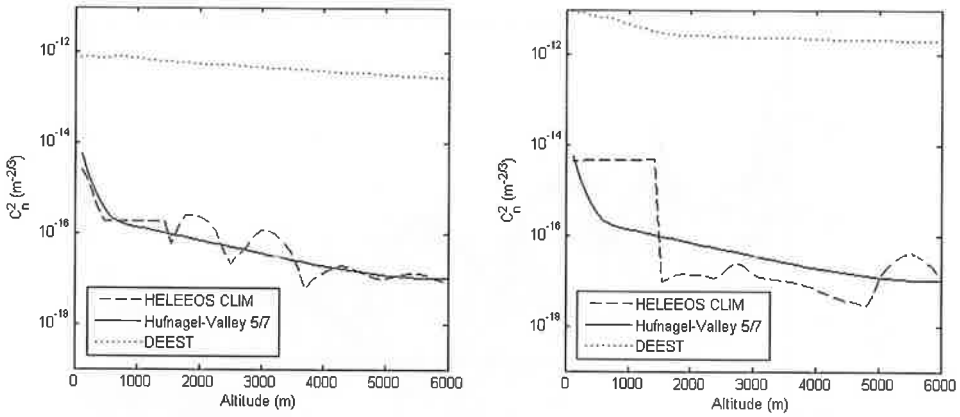

Fig. 6. Comparison of the DEEST optical turbulence profiles for East Asia (left plot) and desert summer (right plot) MM5 data, the CLIM profile for the corresponding ExPERT sites, and the HV 5/7 profile. Note that DEEST has since been updated with a low-altitude correction (Jumper, personal communication, 2007).

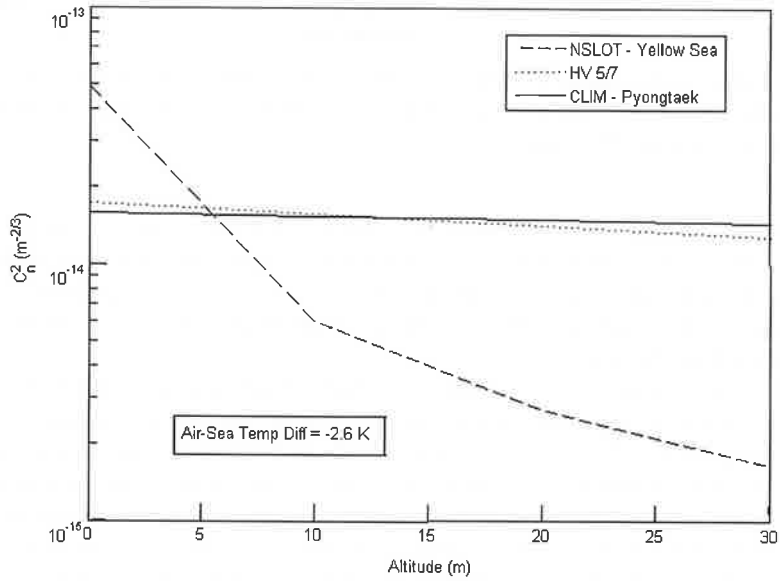

Fig. 7. Optical turbulence profiles for HV 5/7, the winter CLIM profile generated for the ExPERT site Pyongtaek, Korea, and the NSLOT profile for a location off the coast in the Yellow Sea. The geometry for this calculation consists of a platform located at 20 m above the surface, the target at 2 m above the surface, and slant range of 1 km.

over the neighboring ocean. This suggests that both models produce reasonable near-surface C_n^2 values. The slopes of both the HV 5/7 and the CLIM are not the same as that of NSLOT. For the case of the CLIM, this is because the resolution of the profile is not on the order of meters as it is in NSLOT. The CLIM C_n^2 value was determined from the distribution of C_n^2 values from 0 to 66 m.

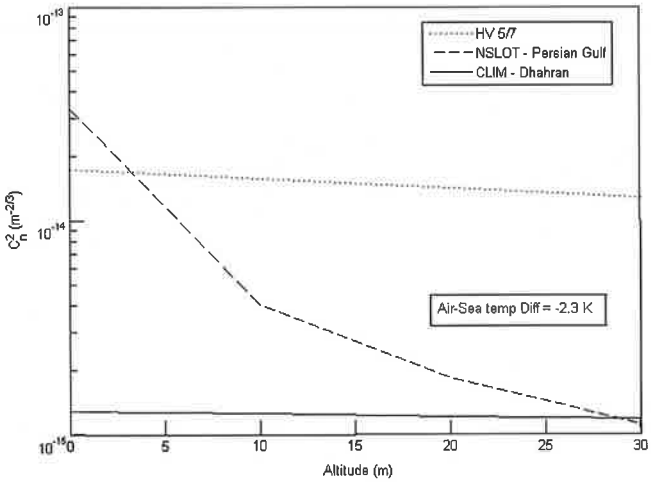

Fig. 8. Optical turbulence profiles for HV 5/7, the CLIM profile generated for the ExPERT site Dhahran, Saudi Arabia, and the NSLOT profile for a location off the coast in the Persian Gulf. The geometry for this calculation consists of the platform located at 20 m above the surface, the target at 2 m above the surface, and slant range of 1 km.

Figure 8 shows the same geometry setup as Fig. 7, but the profiles were calculated for the ExPERT location of Dhahran, Kingdom of Saudi Arabia, and a nearby NSLOT location over the Persian Gulf. This figure also shows a good comparison among the three optical turbulence profiles. Even though the slopes of NSLOT and the CLIM model are not the same in the first 10 m, both profiles predict very similar C_n^2 values from 10 to 30 m.

4.2. Operational implications

The variations in optical turbulence profiles for individual sites noted above have significant effects on modeled HEL system performance, and these differences can be analyzed for individual sites or worldwide. The following figures examine the worldwide changes in HEL system performance prediction between the STD profile of HV 5/7 and the CLIM-derived profile. The CLIM profiles are expected to vary throughout the world since the values of C_n^2 are correlated to RH in the boundary layer, or temperature in the free atmosphere, for a given location's climatology, whereas the HV 5/7 profile produces the same C_n^2 values regardless of the location to which it is applied. Therefore, it is likely that there is a difference in overall Strehl ratio between the two optical turbulence profiles at any given location worldwide. For this paper, overall Strehl ratio is the ratio of energy propagated through all atmospheric effects—extinction, turbulence, thermal blooming—to that of propagation limited only by diffraction. Such changes in expected system performance, when the only differences are due to the different optical turbulence profiles, are illustrated in Fig. 9. The engagement scenario for Fig. 9 has the platform at the top of the boundary layer (1,525 m) and the target on the ground. Therefore, the optical turbulence values for altitudes near the top of the boundary layer and the differences in C_n^2 values between the two profiles at this location play significant roles in the outcome of the Strehl ratio plot for each profile.

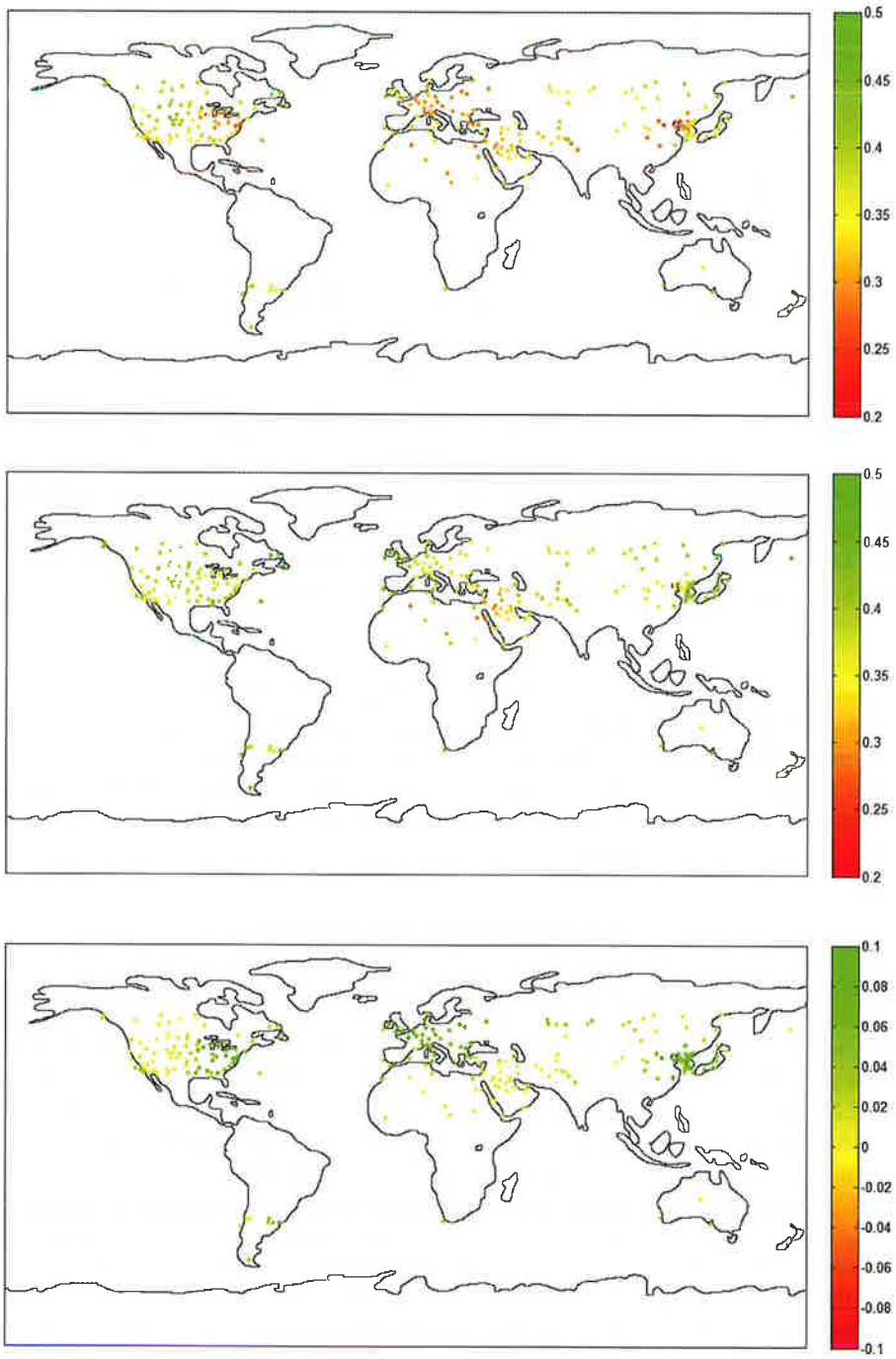

Fig. 9. Worldwide map of Strehl ratio for all ExPERT midlatitude and desert sites for the summer season, 1.06-μm laser wavelength, 50th RH percentile, and downward-looking 4,000-m slant range through the boundary layer: HV 5/7 (top), CLIM (middle), and CLIM – HV 5/7 difference (bottom).

The color bars for the first two maps indicate the Strehl ratio, where the green indicates a higher Strehl ratio of 0.5 and the red a lower Strehl ratio of 0.2. For the last map the color bar indicates the difference in overall Strehl ratio between the CLIM model and HV 5/7. Yellow indicates that the two models yield roughly the same Strehl ratio, and therefore the color has a value of 0. The greener dots indicate that the CLIM model's Strehl ratios were higher than HV 5/7, and vice versa for the red points.

Although the Strehl ratio plots for the HV 5/7 and CLIM look almost the same, there are differences between the two. These differences are also what one would expect according to the analysis above. At the top of the boundary layer, the summer midlatitude profile and HV 5/7 are very similar in value, and therefore, the difference in Strehl ratio is approximately zero. As for the desert region, the summer CLIM profile is slightly larger than HV 5/7. Thus, the scenario using the CLIM profile resulted in a lower Strehl ratio.

Figure 10 illustrates the impact that slant range has on Strehl ratio. The effects due to the differences in C_n^2 profiles are amplified over a longer slant range, and this is evident in Fig. 10 for downward-looking slant ranges of 4,000 and 10,000 m from the top of the boundary

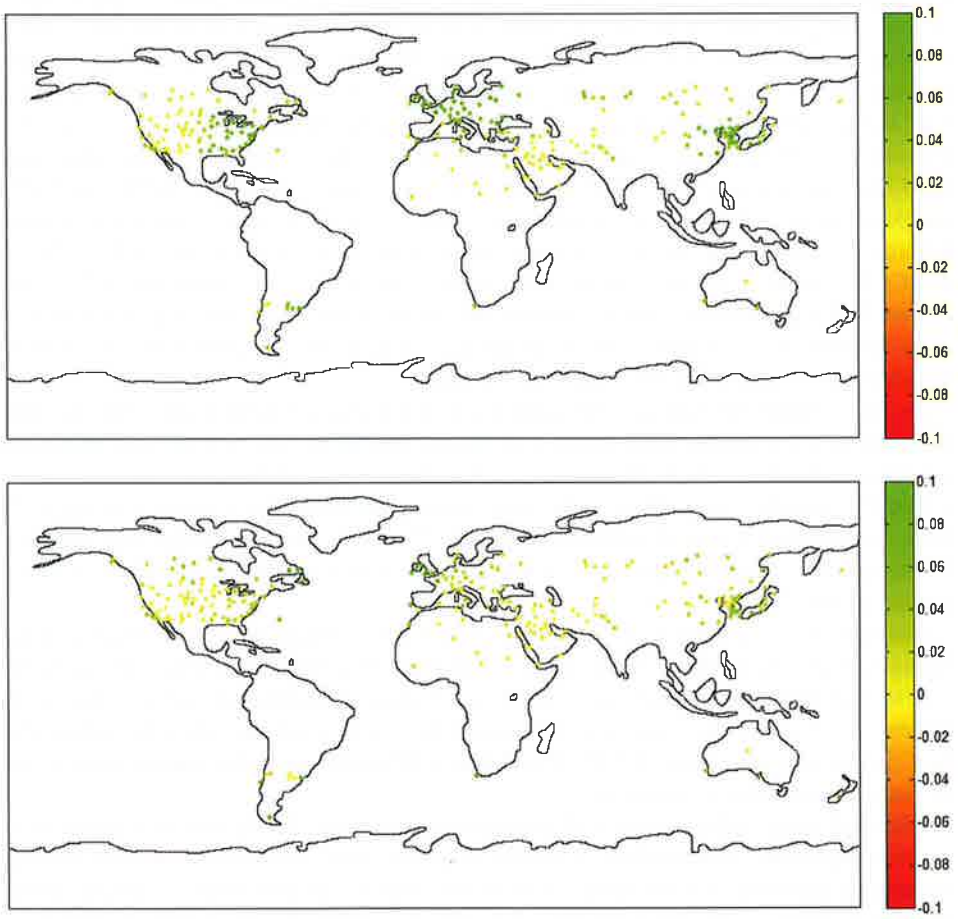

Fig. 10. Strehl ratio difference plots between the CLIM and HV 5/7 profiles for boundary-layer slant ranges of 4,000 m (top) and 10,000 m (bottom).

layer. For the 4,000-m slant range, the difference between the two profiles for midlatitude regions is negligible, but for the 10,000-m slant range there is a considerable change in predicted HEL system performance. This effect varies among ExPERT sites worldwide. In most cases, the CLIM profile predicts a worst-case scenario, but there are locations where the HV 5/7 profile predicts the lower Strehl ratio. Lower Strehl ratios indicated longer required dwell times and shorter expected ranges to achieve the desired effect. These plots show that it is important for future operational HEL weapons risk assessment studies to carefully consider how optical turbulence is characterized for different locations because the various C_n^2 profiles can force significant differences in the predicted performance of a HEL system.

5. Conclusions

This research confirms that there are differences among the available STD, STAT, NUM, and CLIM profiles, which can produce differences in expected HEL system performance not only locally but on a worldwide scale. The magnitude of the variation in performance also depends upon the scenario. For tactical low-altitude, boundary-layer scenarios over a 10-km slant path, the Strehl ratio differences between the CLIM and STD models range from approximately 0.1 to −0.1 (see Figs. 1 and 10). This suggests that the CLIM model predicts shorter required dwell times in some places and longer ones in others than the STD model. These required dwell time differences are on the order of several seconds. For the surface-layer scenario, which was restricted to less than 20 m over a 5-km slant path, the differences in predicted C_n^2 values were quite small among the STD, NUM, and CLIM profiles compared. In terms of system performance, such differences would result in small differences in predicted Strehl ratio and/or required dwell times. However, both the NUM and CLIM profiles can vary with location, time of day, and season, while the STD model cannot. It is important to properly characterize optical turbulence vertical profiles because these differences in profiles—due to geography, time of year, and time of day—can be significant with regard to HEL system performance.

As the comparison between the statistically randomized CLIM model and the thermosonde data showed, the randomization technique used in the STAT model's programming did not completely mimic the fluctuations in the physical data, although it was most similar within the boundary layer. Despite this shortcoming, the randomized profiles appear to be more realistic than a smooth generalized profile. Therefore, using a randomized profile in an engagement scenario might yield a more realistic system performance prediction than a smooth profile.

Unlike the STAT comparison, the purpose of the NUM comparisons was to observe similar magnitudes and distribution shapes in the C_n^2 profiles. The NSLOT comparisons show that even though the model comparison scenarios used different but adjacent surfaces, the profile values are still within the same order of magnitude. These results are taken to confirm that the C_n^2 modeling techniques of NSLOT and the CLIM model are valid characterizations for the input climatological conditions.

Although many different types of comparisons are made throughout this paper, there are two important confirmations from this research. First, this study demonstrates that the optical turbulence CLIM model used by HELEEOS can effectively correlate optical turbulence values to other meteorological parameters, especially RH within the boundary layer. Thus, HELEEOS can produce C_n^2 profiles in a realistic manner that varies with time of day and season. Since the data were sorted by climatological parameters, they are also

applicable to other areas of the world with similar climatology. The HELEEOS CLIM can additionally produce C_n^2 profiles for cases other than the 50th-percentile case, thus quantifying the likelihood of a more extreme profile, such as the 95th-percentile case. Second, the effects due to the differences in optical turbulence models can be calculated using HELEEOS, and the impacts of those differences can be quantified. As an example, the CLIM model could be used to quantify the probability of occurrence of a common STD model such as "2 times CLEAR1" for a given location and time. The understanding and knowledge of the magnitude of these optical turbulence model differences is important because they could have significant operational performance implications for HEL weapons systems such as the Airborne Laser and Advanced Tactical Laser.

6. Acknowledgments

The authors recognize the outstanding support of the High Energy Laser Joint Technology Office, Albuquerque, New Mexico, and two reviewers whose comments, suggestions, and critical insights significantly improved the paper. The views expressed in this paper are those of the authors and do not necessarily reflect the official policy or position of the Air Force, the Department of Defense, or the U.S. Government.

References

[1] Alliant Techsystems Mission Research, "ATMtools: A Toolbox for Atmospheric Propagation Modeling. Users Guide Version 2.4," Mission Research Document ATK/MR-DN-R-05-04, 27 September 2005.

[2] Beland, R.R., "Propagation Through Atmospheric Optical Turbulence," in *Atmospheric Propagation of Radiation*, edited by F.G. Smith, pp. 157–232, SPIE, Bellingham, WA (1993).

[3] Bussey, A.J., J.R. Roadcap, R.R. Beland, and G.Y. Jumper, "Master Data Base for Optical Turbulence Research in Support of Airborne Laser, Air Force Research Laboratory Technical Report, AFRL-VS-TR-2000-1545. 2000.

[4] Fiorino, S.T., R.J. Bartell, G.P. Perram, D.W. Bunch, L.E. Gravley, C.A. Rice, Z.P. Manning, and M.J. Krizo, J. Directed Energy **1**(4), 347 (2006).

[5] Frederickson, P.A., K.L. Davidson, C.R. Zeisse, and C.S. Bendall, J. Appl. Meterol. **39**, 1770 (2000).

[6] Gravley, L.E. "Comparison of Climatological Optical Turbulence Profiles to Standard, Statistical and Numerical Models using HELEEOS" M.S. Thesis, Air Force Institute of Technology, March 2006.

[7] Hufnagel, R.E. "Propagation Through Atmospheric Turbulence," *The Infrared Handbook*, edited by W.L. Wolfe and G.J. Zissis, Infrared Information Analysis Center, Ann Arbor, MI (1985).

[8] Jumper, G.Y., J.R. Roadcap, S.C. Adair, G.P. Seeley, and G.T. Fairley, J. Directed Energy **1**(3), 183 (2005).

[9] Koepke, P., M. Hess, I. Schult, and E.P. Shettle, "Global Aerosol Data Set," Max Planck Institute Meteorologie Hamburg Report 243, 1997.

The Authors

Mr. R. J. Bartell received his B.S. degree in physics from the U.S. Air Force Academy as a distinguished graduate in 1979. He received his M.S. degree from the Optical Sciences Center, University of Arizona, in 1987. He is currently a Research Physicist with the Center for Directed Energy at the Air Force Institute of Technology, where he leads the development of the High Energy Laser End-to-End Operational Simulation (HELEEOS) model.

Lt. Col. Steven Fiorino is an Assistant Professor of atmospheric physics at the Air Force Institute of Technology (AFIT) and a research faculty member within AFIT's Center for Directed Energy. He has B.S. degrees from Ohio State (1987) and Florida State (1989) universities, an M.S. in atmospheric dynamics from Ohio State (1993), and a Ph.D. in physical meteorology from Florida State (2002). His research interests include microwave

remote sensing, development of weather signal processing algorithms, and atmospheric effects on military systems such as high-energy lasers and weapons of mass destruction.

Ms. Liesebet Gravley graduated from Wittenberg University in 2004 with a Bachelor of Arts in physics and German. During the summer of 2004, she was hired as a Directed Energy Professional Society (DEPS) intern, where she did research on characterizing optical turbulence. She continued at AFIT as a civilian masters student, graduating in March 2006. Currently, she is an English and physics instructor in Slovakia.

Mr. Matthew Krizo is currently the lead programmer for the HELEEOS project as part of AFIT's Center for Directed Energy. He has been working with HELEEOS since 2004. He oversees the development of the model and the incorporation of new capabilities into HELEEOS. He received a B.S.E.E in 2005 from Cedarville University. He is currently working on an M.S.E.E from the University of Dayton and is expected to graduate in spring of 2008.

Ms. Kelly Le was an undergraduate research assistant within AFIT's Center for Directed Energy during the period of this research project.

Dr. Glen Perram received his B.S. degree in applied physics from Cornell University in 1980 and his M.S. and Ph.D. degrees in physics from the Air Force Institute of Technology in 1981 and 1986, respectively. He is currently Professor of Physics at AFIT, having served as a member of the faculty since 1989. Professor Perram's research interests include chemical lasers, remote sensing, optical diagnostics, and laser weapons systems modeling.